Electronic Supplementary Material (ESI) for Physical Chemistry Chemical Physics.
This journal is © the Owner Societies 2017

Mechanism of ultrafast non-reactive deactivation of the retinal chromophore in non-polar solvents

M. Mališ,[a,b] J. Novak,[a] G. Zgrablić,[c,d] F. Parmigiani[c,e,f] and N. Došlić[a]

[a] Department of Physical Chemistry, Ruđer Bošković Institute, Bijenička cesta 54, 10000 Zagreb, Croatia
[b] Centre Européen de Calcul Atomique et Moléculaire, École Polytechnique Fédérale de Lausanne, Avenue Forel 2, 1015 Lausanne, Switzerland
[c] Elettra-Sincrotrone Treste, T-ReX Laboratory, Strada Statale 14 - km 163,5 in AREA Science Park 34149 Basovizza, Trieste, Italy
[d] Politehnika Pula, Riva 6, 52000 Pula, Croatia
[e] Department of Physics, Università degli Studi di Trieste, I-34127 Trieste, Italy
[f] International Faculty, University of Cologne, Albertus-Magnus-Platz 50923 Cologne, Germany

Supporting Information

S1.Ground state dynamics

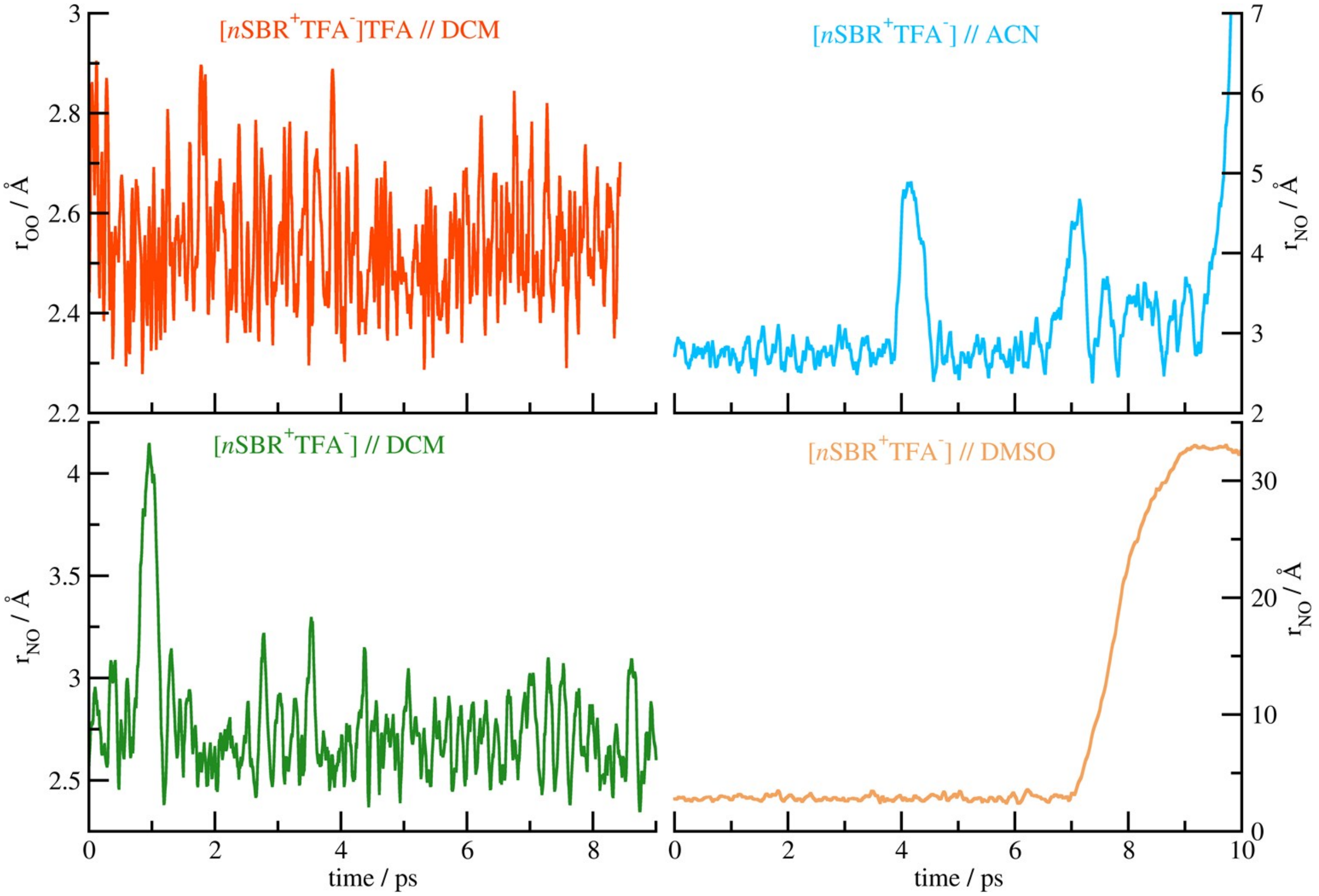

Figure S1. Evolution of the nonbonding O···O and N···O distance during the ground state trajectory of the [nSBR$^+$TFA$^-$]TFA and [nSBR$^+$TFA$^-$] in DCM, ACN and DMSO showing the dissociation of the ion-pairs in ACN and DMSO.

S1. Experimental methods

The *n*-butylamine Schiff base of all-*trans* retinal was prepared according to previously described methods[1] and protonated using a one to five-fold excess of trifluoroacetic acid. The solutions were prepared starting from pure dried dichloromethane (DCM) or dimethyl sulfoxide (DMSO) and used as received.

The sample steady-state absorption between 300 nm and 600 nm was measured by mean of a commercial spectrophotometer (Pharmacia Biotech Ultraspec 3000). The optical density (OD) measured at the absorption maximum (465 nm), for a 1 mm thick sample, was 0.75–0.9. A 1 kHz regenerative amplifier was used to generate 50–60 fs pulses at 800 nm with an energy of ~0.6 mJ. By focusing a portion of the fundamental beam to a 2 mm thick CaF_2 crystal a supercontinuum (SC) white light from 350 to 950 nm was generated. The SC beam was split into the probe and the reference beam by using a metallic-coated beamsplitter. The probe beam alone was imaged onto the sample to a spot of a ~70 μm diameter and it was in spatial-temporal coincidence with the pump at 400 nm having spot size on the sample $\geq$140 μm. Before arriving on the sample the pump beam was chopped at 250 Hz. The probe and the reference beams were then dispersed, after the interaction with the sample, on two 512 pixel diode arrays with a homemade spectrometer based on transmission grating. The diode arrays were integrating signals from two consecutive pulses while control software first sorted acquired spectra into the pumped and the unpumped group, and then each group was averaged out. For each time step 2000 shots were used. All the beams had identical polarization. The pump-probe delay was varied independently by mean of motorized translation stage. Cross correlation of ~85 fs across the full spectral range and group velocity dispersion were obtained by observing non-resonant cross-phase modulation signal obtained from the pump-probe scans in pure solvent and thus instrumental response function (IRF) was determined. The intensity of the 400 nm pump (~135 μW) was chosen to achieve the linearity of the pump-probe signal, i.e. variation of the optical density ΔOD. By using a peristaltic pump the sample was circulated through quartz capillary (Vitrocom, 0.5 mm pathlength, 0.25 mm quartz window). The flow speed was chosen to ensure sample refreshment for each laser pulse.

Transient absorption spectra. Figures S1 and S2 show transient absorption spectra of the [*n*SBR$^+$TFA$^-$] ion pair (chromophore-counterion ratio 1:1) in non-polar DCM and highly polar DMSO, respectively. Scattering of the pump beam in the sample and quartz capillary is responsible for spikes and high noise in the region around 400 nm. On the red part of the spectrum there are oscillatory features that span region from 770 to 840 nm. These artefacts appear because intensity of the probe beam in the region around the 800 nm fundamental increases too steeply which makes calculation of the differential optical density (ΔOD) less reliable.

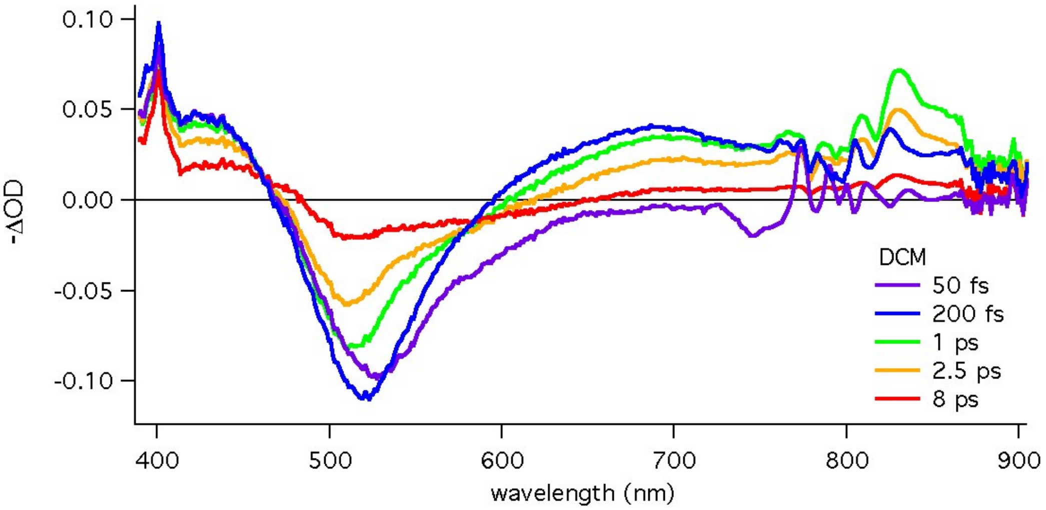

Figure S2. Transient absorption spectra of the [*n*SBR$^+$TFA$^-$] ion pair in DCM for various delay times. Excitation was at 400 nm.

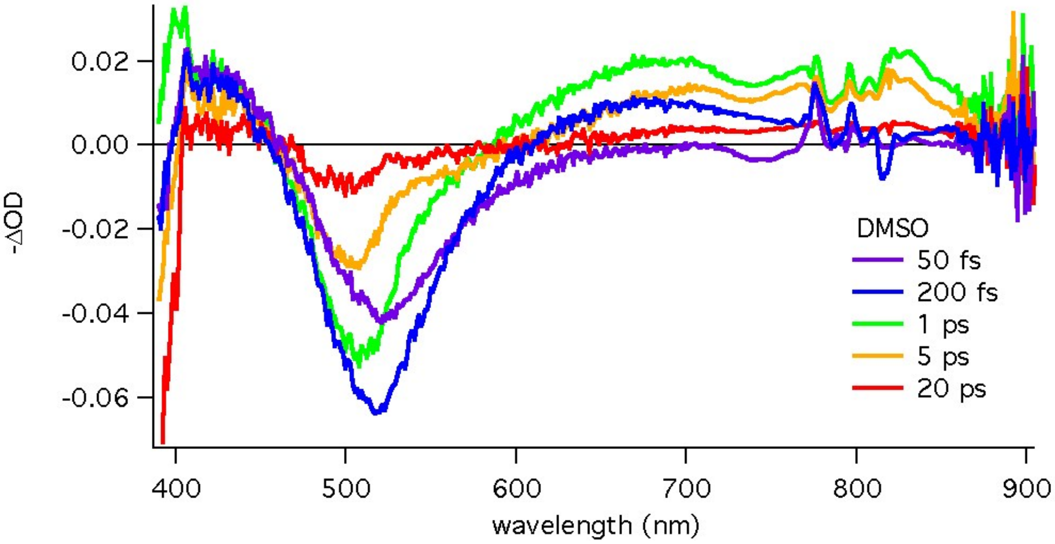

Figure S3. Transient absorption spectra of the *n*SBR$^+$ in DMSO for various delay times. Excitation was at 400 nm.

Although on the picosecond timescale one finds three times slower dynamics in DMSO compared to DCM, within the first few hundred femtoseconds in both solvents the spectral features and their dynamics are qualitatively similar to the ones found in earlier studies for [*n*SBR$^+$TFA$^-$]TFA ion pair in ethanol[1–3] where chromophore-counterion ratio (CC ratio) was more than 1:2. These spectral features are:

- excess transmission that peaks at 430 nm, appears instantaneously and is caused by reactant bleaching;
- excess absorption that peaks around 510 nm, appears simultaneously with the excess transmission and is assigned to an excited state absorption. Although it peaks at 510 nm, the excited state absorption extends down to 950 nm[2];
- within 200 fs the excess transmission above 600 nm develops and is assigned to excited state fluorescence, i.e. stimulated emission in case of the pump probe measurements[1–5]. The excited state absorption rises again between 700 and 800 nm (see spectrum at 50 fs, Fig. S1 and S2) where it partially cancels intensity of the stimulated emission and causes a broad dip centered around 750 nm[2].

Extraction of stimulated emission decay from pump probe measurements. The aim of experimental part of this study is to determine whether the excited state lifetime of the *n*SBR$^+$ changes when it is titrated with TFA acid to obtain CC ratios of 1:1, 1:2 and 1:4 (1:5 in DMSO). For that purpose, time resolved fluorescence measurements, obtained for example with up-conversion or Kerr effect optical setups, are ideally suited as they are sensitive only to the excited state dynamics. On the other hand, in pump probe measurements both ground and excited state contributions can spectrally overlap and their sum is equal to transient absorption spectra.

As in case of the CC ratio of 1:4 in DCM we have time resolved fluorescence spectra (obtained from the up-conversion setup used in a previous article of one of our contributors[4]) from which is possible to determine whether there exists wavelength and delay range where the pump probe signal is due to the stimulated emission only, i.e. where only the excited state dynamics is observed. From Fig. S1 and S2 it can be observed that spectral range between 650 and 700 nm is the right place to search because there the excess transmission reaches maximum intensity while at the same time the excited state absorption (see spectrum at 50 fs) should be very weak.

Therefore, kinetic traces obtained with our current pump probe setup (PP traces, black curves) and those obtained with the polychromatic fluorescence up-conversion setup (UC traces, red curves) used in[4] were taken at 20 wavelengths between 650 and 700 nm. The traces were then normalized but their original time zero was not adjusted. Figures S4-S6 show selection of 9 pairs of the PP and UC traces (black and red curves, respectively) at wavelengths between 658 and 682 nm together with their difference (blue curve, top panel). It can be observed that from 664 to 676 nm and for delays larger than 1 ps the PP traces, within experimental noise, coincide with the UC traces.

Time resolved fluorescence measurements[4] determined that emission of *n*SBR$^+$ in DCM at 670 nm originates in large extent from vibrationally relaxed S_1 fluorescence (90%), while the remaining intensity is attributed to S_2 fluorescence (6%) and short-lived vibrationally hot S_1 fluorescence (4%). Moreover, no sign of dielectric solvation that would cause dynamic Stokes shift was detected in DCM.

In conclusion, the PP kinetic trace averaged into 670 ± 5 nm range for delays larger than 1 ps reflects relaxation dynamics of the excited states.

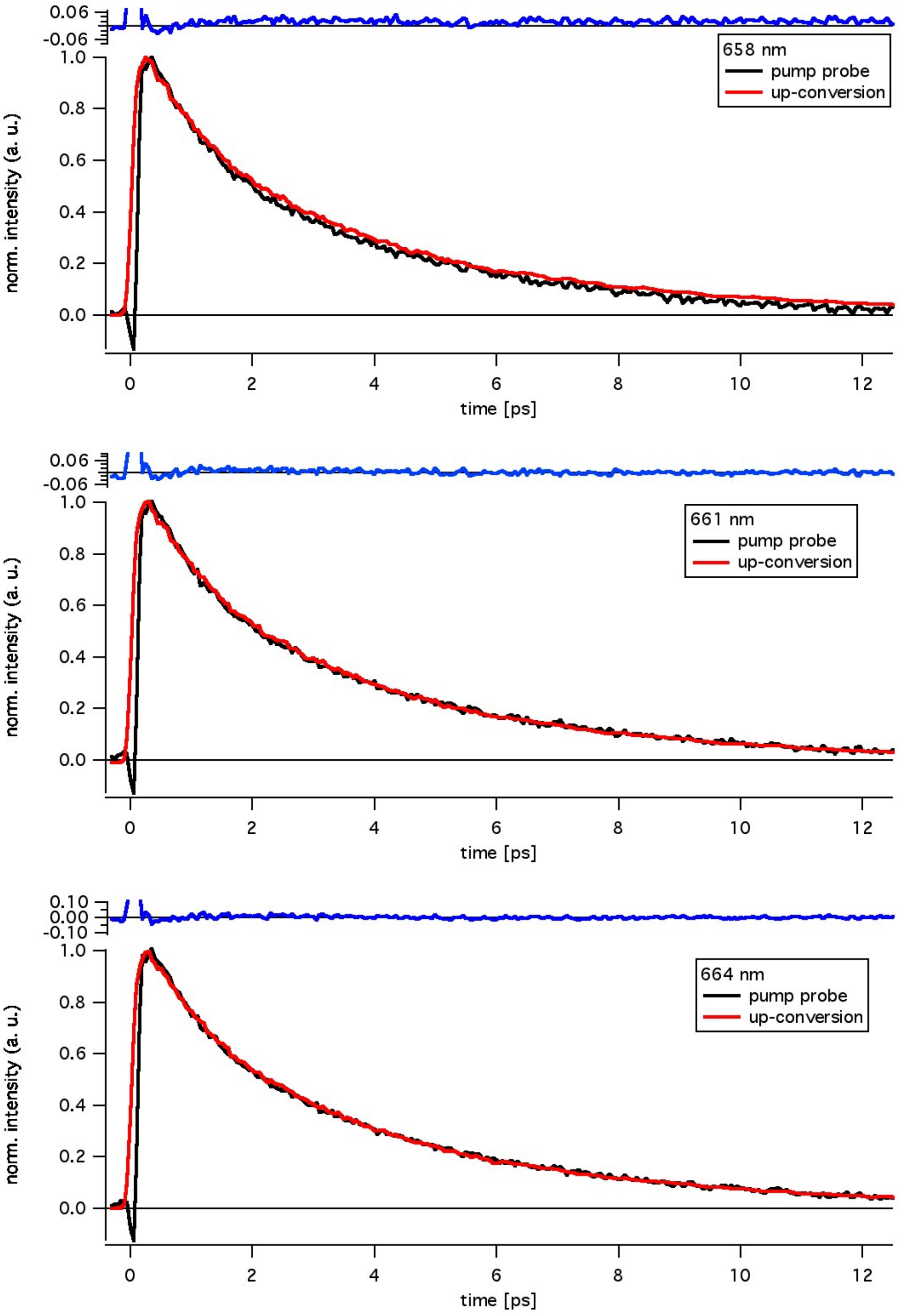

Figure S4. Normalized kinetic traces at 658, 661 and 664 nm obtained with the pump-probe setup (the PP trace, black curve) and the polychromatic fluorescence up-conversion setup (the UC trace, red curve). Top panel in each graph shows difference between the PP and the UC traces (blue curve) and its y-axis has been scaled in order that experimental noise can be evident. As a consequence the blue curve gets cut around *t*=0 fs.

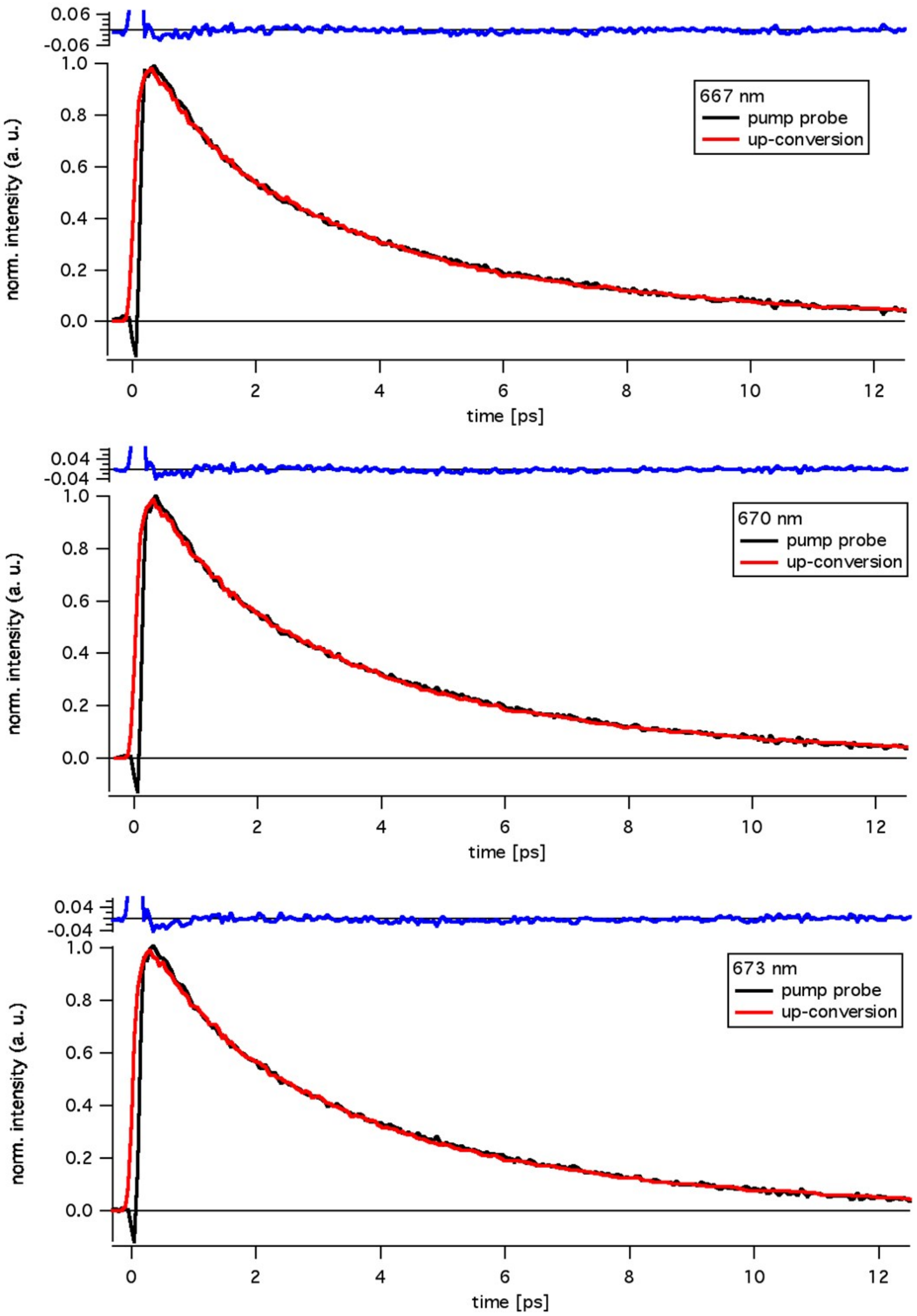

Figure S5. Same as Fig. S4 but for probing wavelengths at 667, 670 and 673 nm.

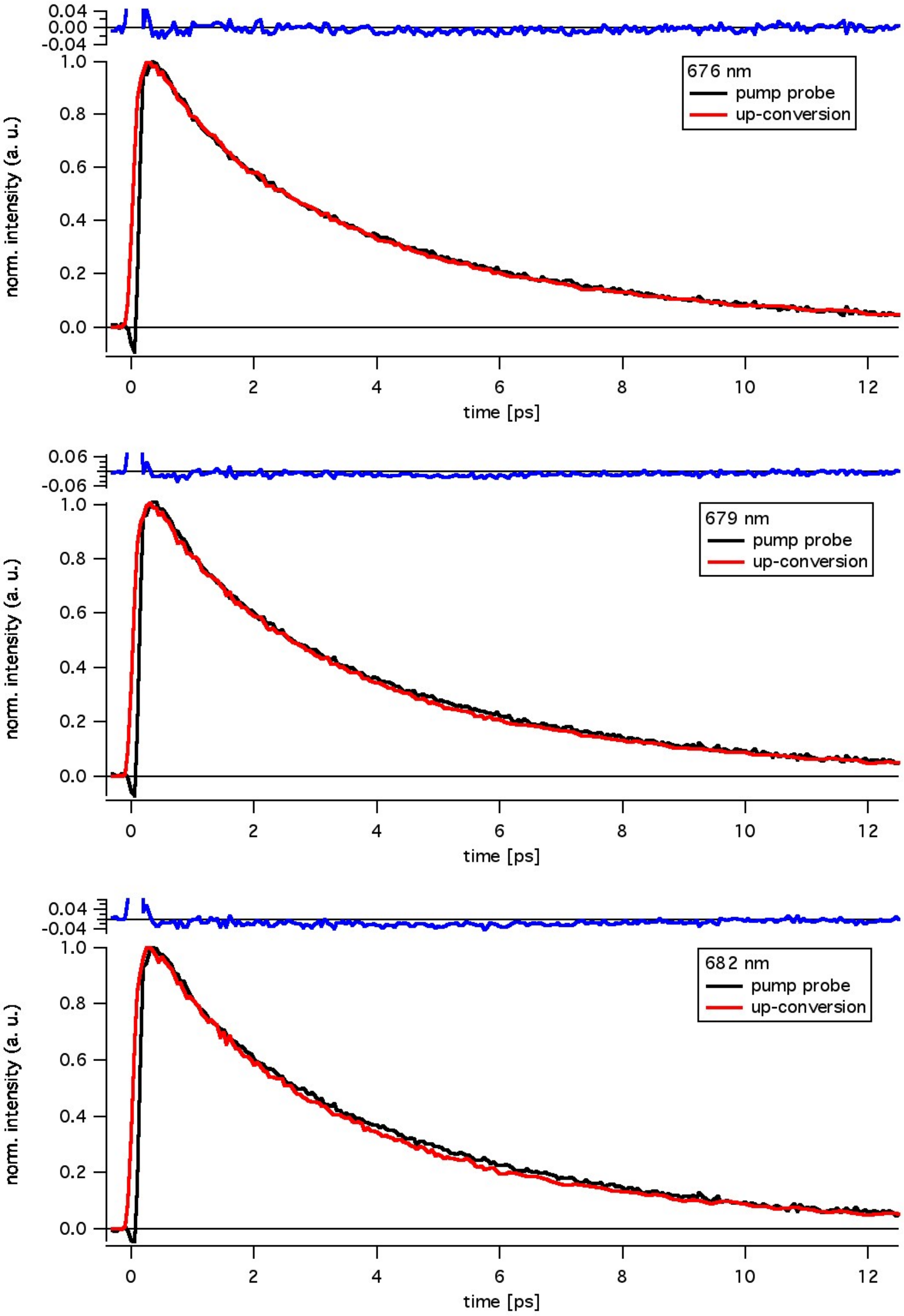

Figure S6. Same as Fig. S4 and S5 but for probing wavelengths at 676, 679 and 682 nm.

Absence of spectral shifts in function of the chromophore-counterion ratio. The previous analysis is valid for CC ratio of 1:4, the only ratio for which time resolved fluorescence spectra were available. Nevertheless, if for a fixed delay the characteristic spectral features do not shift in wavelength as we increase the acid concentration (CC ratios of 1:1, 1:2 and 1:4), the wavelength-delay range where the PP traces coincide with the UC traces will remain the same as in the case of the CC ratio of 1:4.

Indeed, for the *n*SBR$^+$ in DCM maxima of the excess transmission that peaks at 430 nm, the excess absorption that peaks at 510 nm and the excess transmission above 600 nm do not show any spectral shift as the CC ratio is changed from 1:1 to 1:2 and finally to 1:4 (Fig. S7). This is true at all characteristic delay times shown in Fig. S7. It can be concluded that the excited state absorption and the stimulated emission bands do not spectrally shift in function of the CC ratios in range we employed here (1:1 to 1:4).

If these bands were spectrally shifting, it would be necessary to accordingly shift the probing wavelength in order to have equal contribution of the bands. The absence of any spectral shift justifies our choice to keep the probing wavelength fixed for any CC ratio.

For the *n*SBR$^+$ in DMSO the absence of any spectral shift in function of the CC ratio was detected, too. Furthermore, when the time resolved spectra in function of the CC ratio are normalized they, within experimental noise, coincide at all characteristic delay times (Fig. S8). The same is true when the kinetic traces in function of the CC ratio are normalized – they, within experimental noise, coincide at various characteristic wavelengths. In other words, the normalized spectro-temporal matrices in function of the CC ratio coincide within experimental noise. Therefore, the choice of the probing wavelength for the *n*SBR$^+$ in DMSO becomes irrelevant.

Nevertheless, in DMSO we also choose 670 nm for the probing wavelength. Similarity of the transient absorption spectra in these two solvents (Fig. S2 and Fig. S3) assures that the PP kinetic trace averaged into 670 ± 5 nm range for delays larger than 700 fs will very closely reflect relaxation dynamics of the excited states.

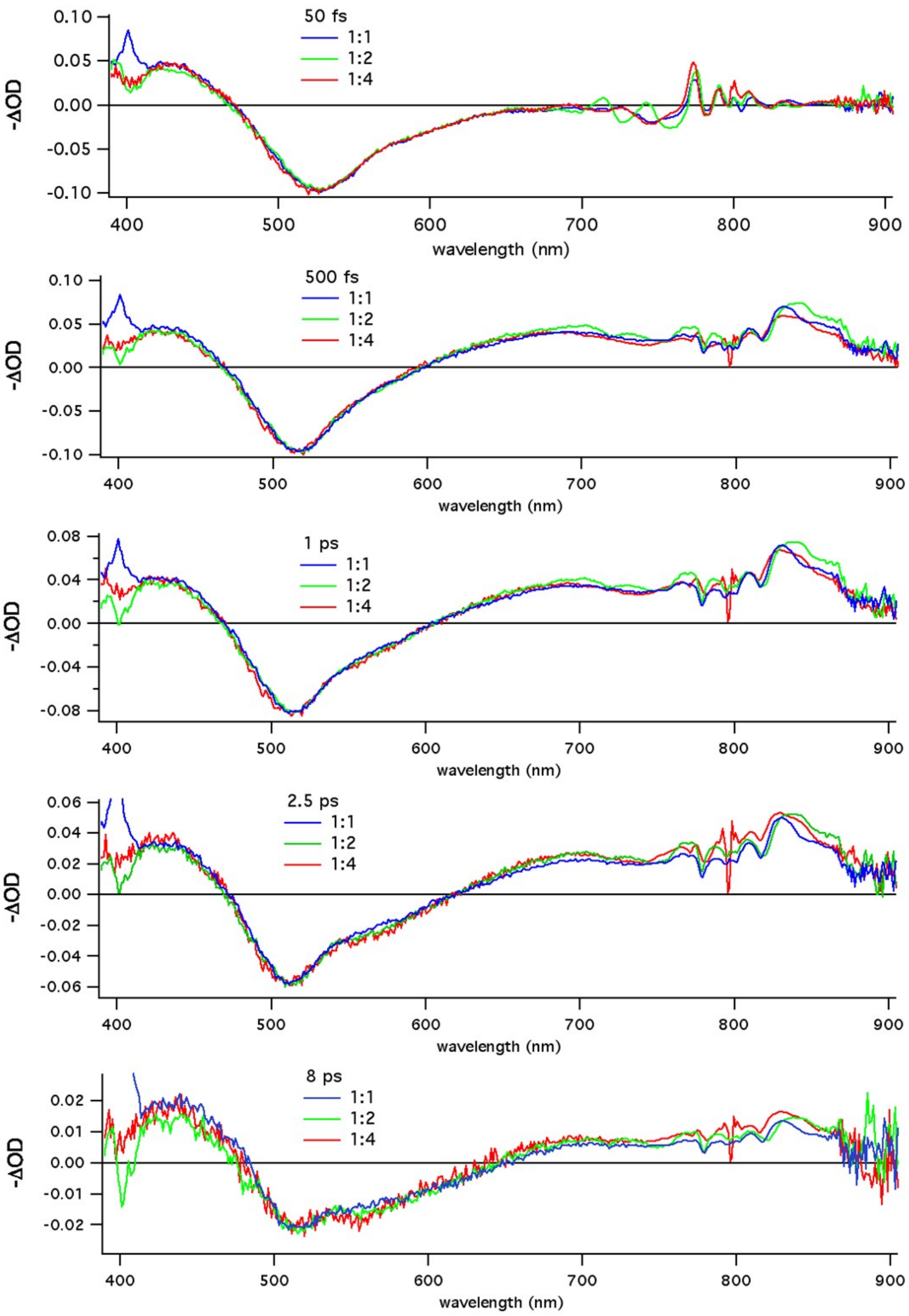

Figure S7. Normalized transient absorption spectra of the *n*SBR$^+$ in DCM for different chromophore-counterion ratios (blue 1:1, green 1:2, red 1:4) at characteristic delay times. Excitation was at 400 nm.

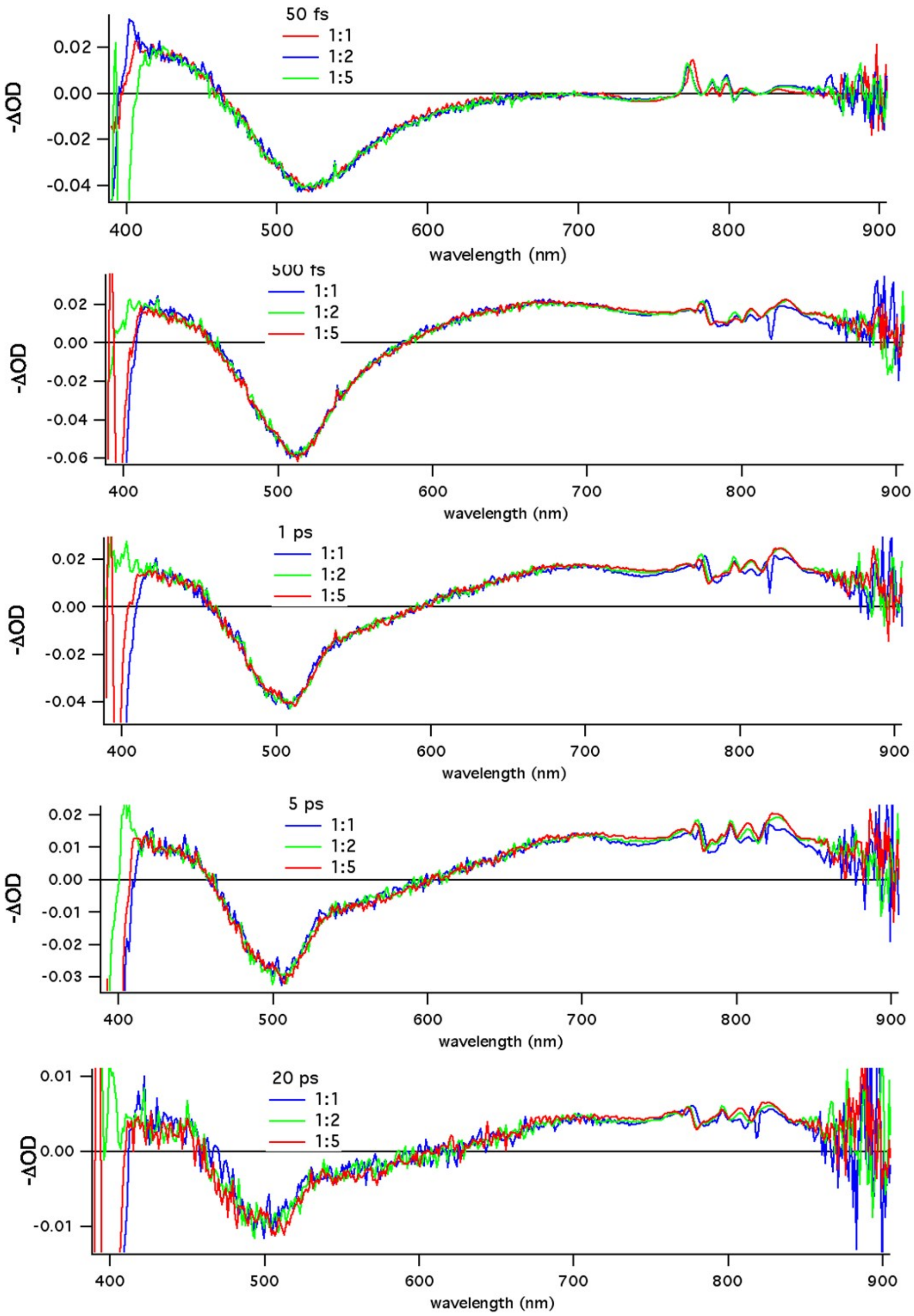

Figure S8. Normalized transient absorption spectra of the *n*SBR⁺ in DMSO for different chromophore-counterion ratios (blue 1:1, green 1:2, red 1:5) at characteristic delay times. Excitation was at 400 nm.

Monoexponential fit of the 670 nm probing wavelength. The PP kinetic trace averaged over the 670 ± 5 nm range was fitted with a monoexponential function for delays larger than 1 ps as only after that time delay it reflects relaxation dynamics of the excited states. Although literature reports that excited state dynamics of SBR$^+$ is multiexponential[1-5], we refrain from using multiexponential fitting function as from our pump probe measurements it is not possible to assess the excited state dynamics before 1 ps. Nevertheless, the monoexponential fits are useful as they give information on how the average lifetime changes with the CC ratio.

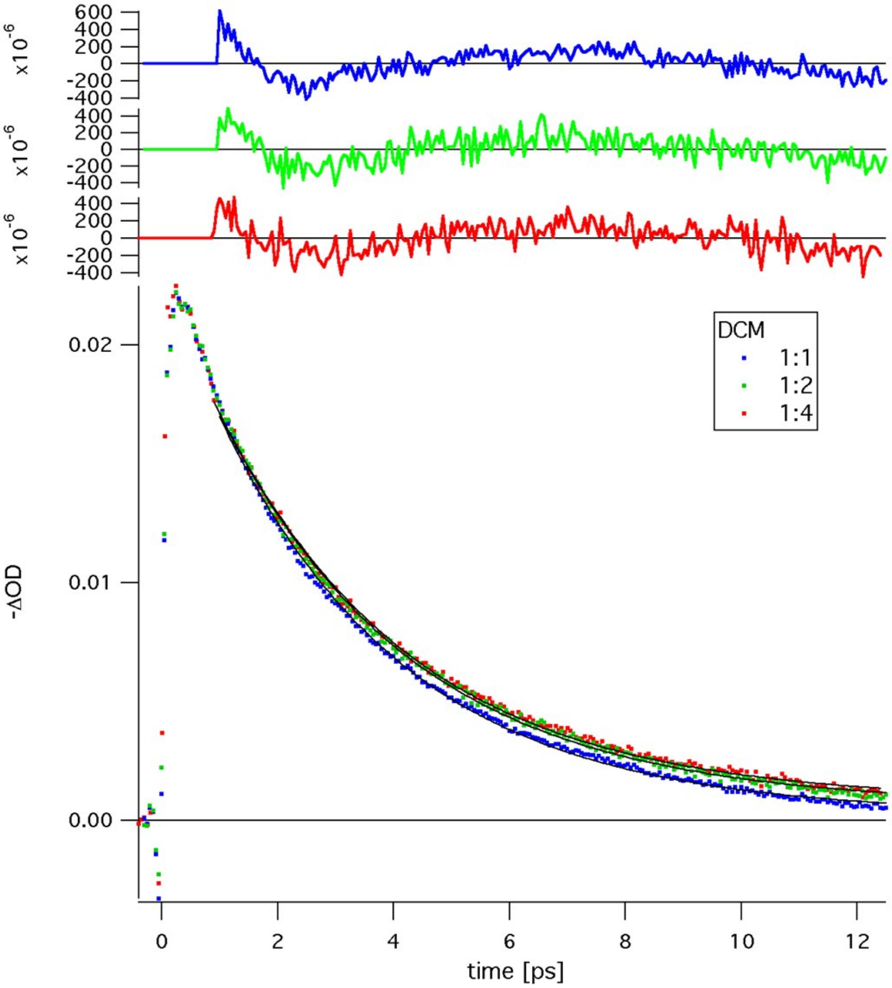

Figure S9. The normalized PP kinetic traces averaged over the 670 ± 5 nm range for three chromophore-counterion ratios (dots), their monoexponential fit for delays larger than 1 ps (black curves) and fit residuals (top panels: 1:1 blue, 1:2 green, 1:4 red). The solvent is DCM.

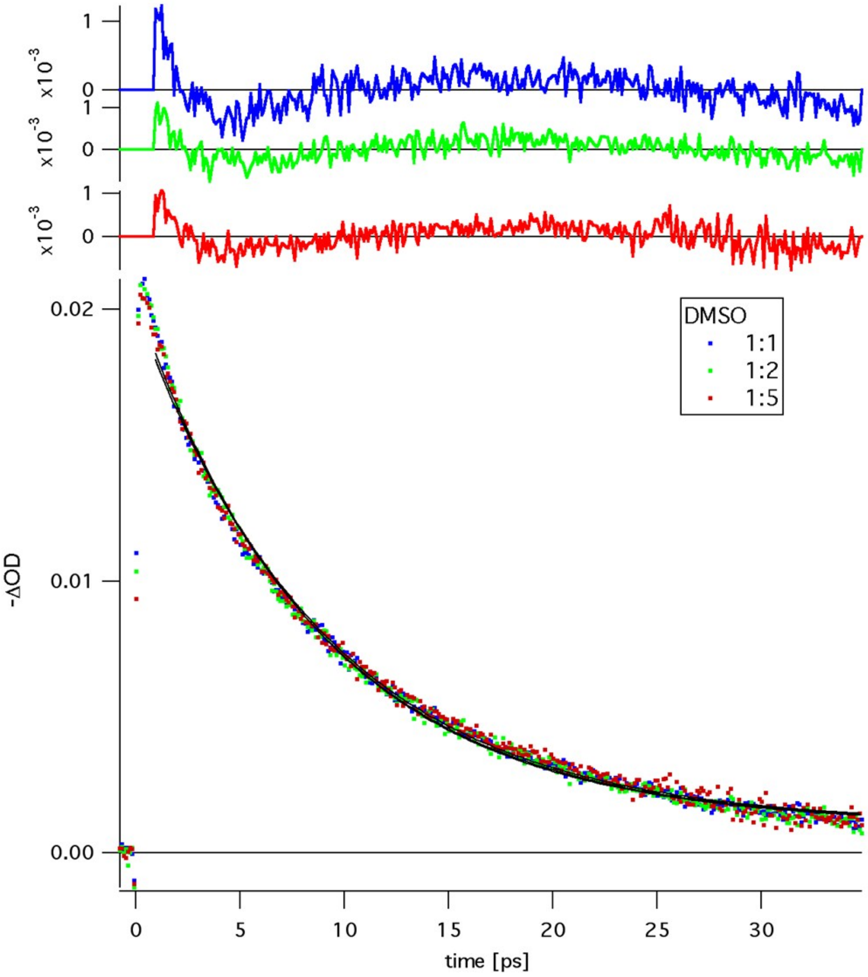

Figure S10. The normalized PP kinetic traces averaged over the 670 ± 5 nm range for various chromophore-counterion ratio (dots), their monoexponential fit for delays larger than 1 ps (black curves) and fit residuals (top panels: 1:1 blue, 1:2 green, 1:5 red). The solvent is DMSO.

The decay constants of monoexponential fits (Table S1) reveal that the average excited state lifetime slows down by 120 fs for the *n*SBR$^+$ in DCM in going from the CC ratio of 1:1 to 1:2. Change in the CC ratio from 1:2 to 1:4 doesn't show any change in the decay constant. In DMSO the average excited state lifetimes don't show any trend with increasing CC ratio from 1:1 to 1:5 and, within fit uncertainty, these lifetimes remain constant.

Table S1. The decay constants of monoexponential fits (in fs) from Fig. S8 and S9.

chromophore-counterion ratio	**DCM**	**DMSO**
1:1	3240±20	8950±80
1:2	3355±25	8800±80
1:4	3360±20	—
1:5	—	9090±80

(1) Hamm, P.; Zurek, M.; Röschinger, T.; Patzelt, H.; Oesterhelt, D.; Zinth, W. *Chem. Phys. Lett.* 1996, **263**, 613.

(2) Bismuth, O.; Friedman, N.; Sheves, M.; Ruhman, S. *Chem. Phys.* 2007, **341**, 267.

(3) Hou, B.; Friedman, N.; Ruhman, S.; Sheves, M.; Ottolenghi, M. *J. Phys. Chem. B* 2001, **105**, 7042.

(4) Zgrablić, G.; Haacke, S.; Chergui, M. *J. Phys. Chem. B* 2009, **113**, 4384.

(5) Zgrablić, G.; Voïtchovsky, K.; Kindermann, M.; Haacke, S.; Chergui, M. *Biophys. J.* 2005, **88**, 2779.

S3.Excited state analysis

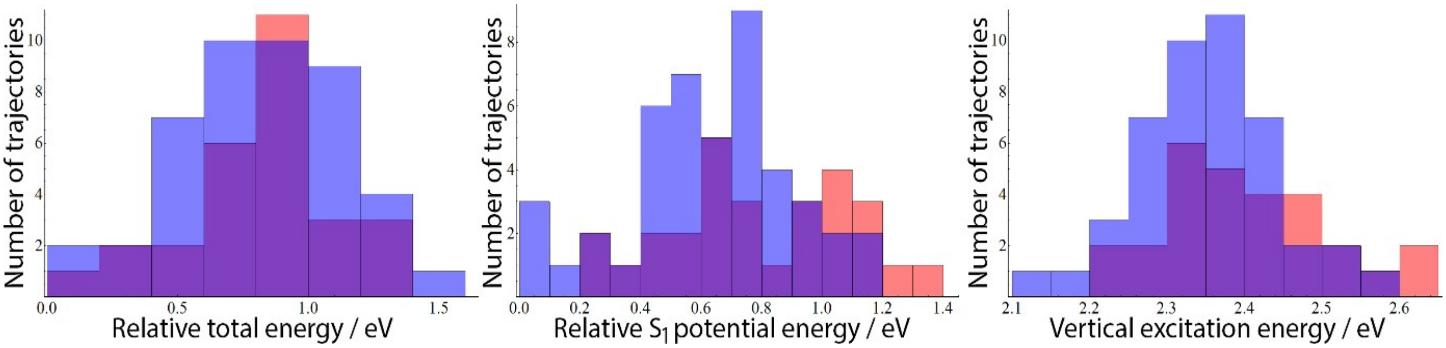

Figure S11. Distribution of the total energy for the initial geometry in all trajectories (right), S1 excited state potential energies (centre) and vertical excitation energies (left) for the [*n*SBR$^+$TFA$^-$]TFA system. Trajectories that deactivate and those that do not deactivate to the ground electronic state in the simulation time are designated with red and blue columns, respectively. The relative energies are to the corresponding smallest values in the two sets.

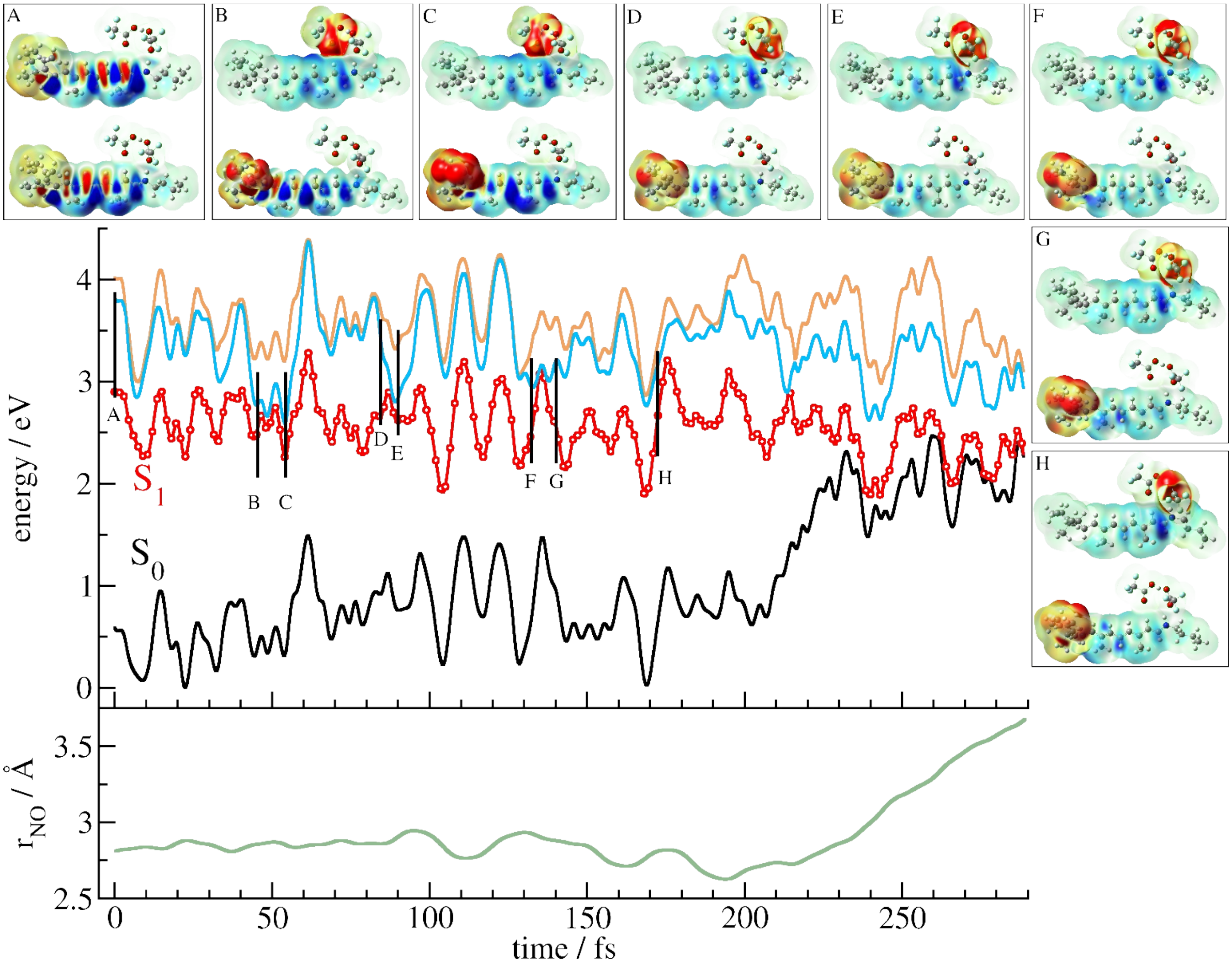

Figure S12. Analysis of the non-reactive relaxation of [*n*SBR$^+$TFA$^-$]TFA in DCM from Figure 3. Additional electron density differences for S_1 and S_2 states along trajectory are shown in insets.

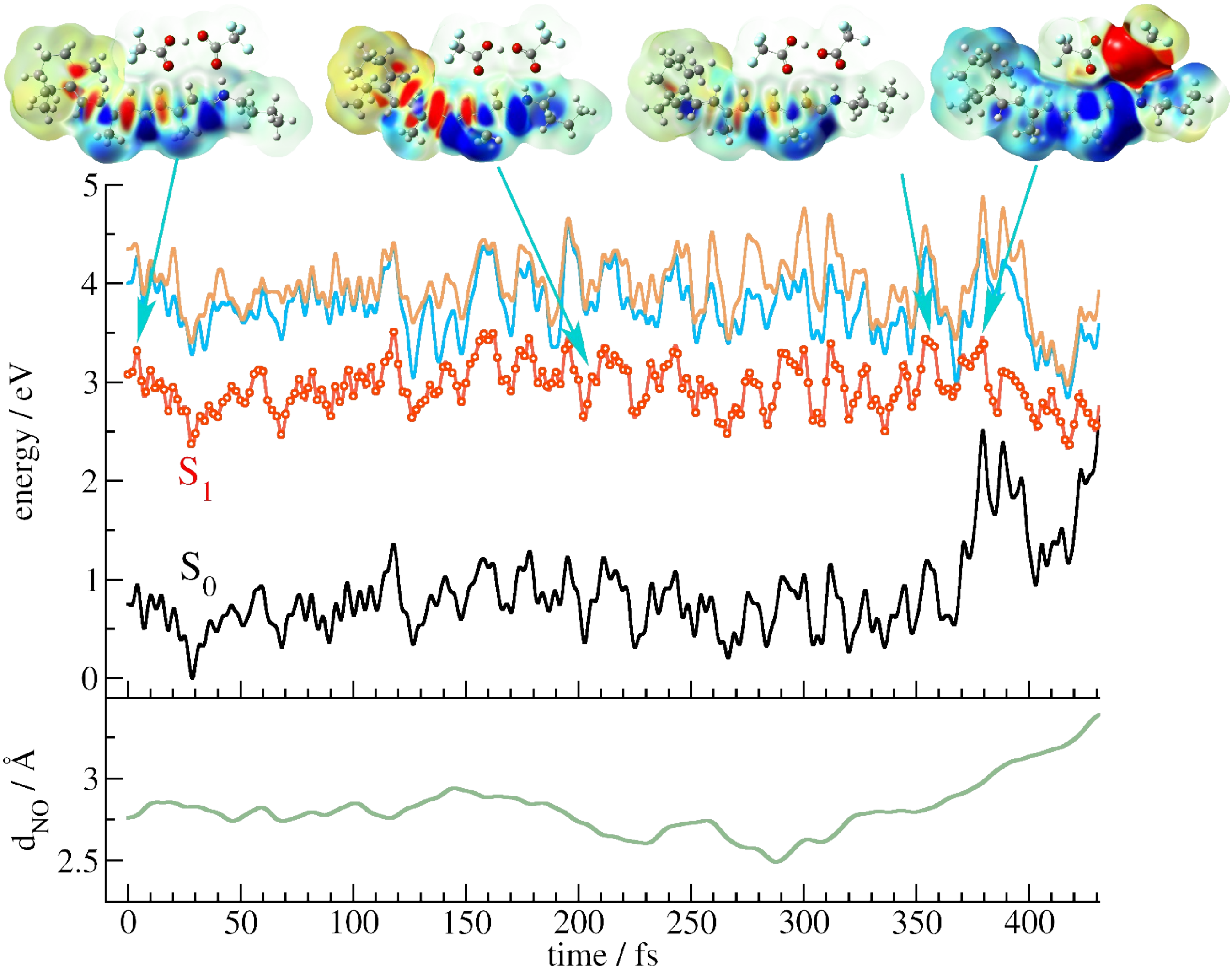

Figure S13. Non-reactive relaxation of [*n*SBR$^+$TFA$^-$]TFA in DCM driven by the conical intersection between the intra-CT and inter-CT states. (a) Time dependence of the potential energy of the electronic ground state (S_0, black) and the first two excited singlet states (S_1, red; S_2, blue) for the selected nonadiabatic trajectory. The circles indicate the populated state at a given time. The insets show the electron density difference of the S_1 and S_0 states with areas of depletion (increase) of electron density in S_1 shown in red (blue). The character of the S_1 state changes from ππ* (left) to intra-CT (middle) and inter-CT (right). The switch from intra-CT to inter-CT state at 367 fs is followed by the dissociation of [*n*SBR$^+$TFA$^-$]TFA. (b) Steep increase of the chromophore-counterion distance, d_{NO} on the inter-CT state. The computations have been performed at the PBE0/SVP//GAFF level, for details see Computational Methods.

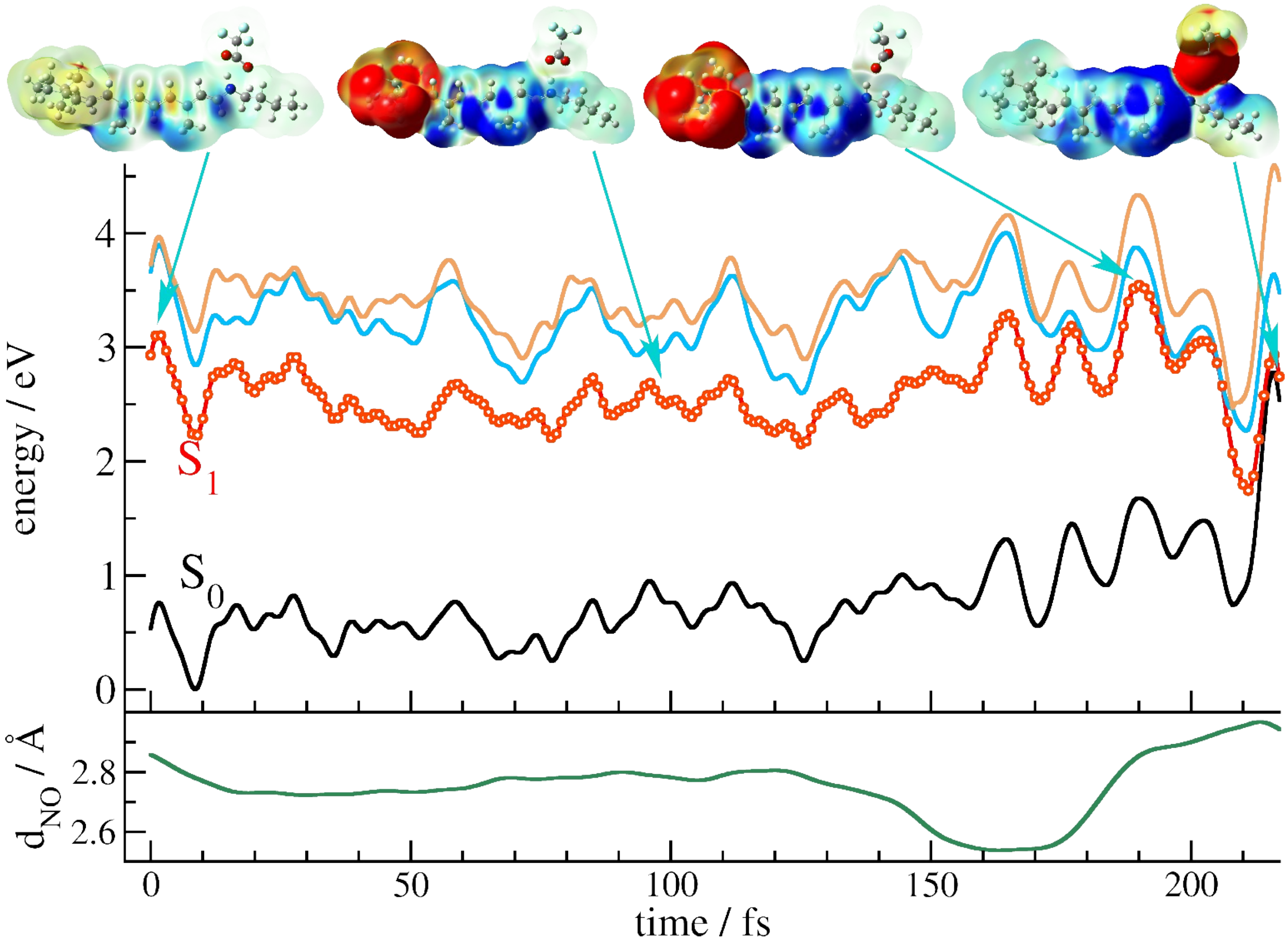

Figure S14. Non-reactive relaxation of [*n*SBR$^+$TFA$^-$] in DCM driven by the conical intersection between the intra-CT and inter-CT states. (a) Time dependence of the potential energy of the electronic ground state (S_0, black) and the first two excited singlet states (S_1, red; S_2, blue) for the selected nonadiabatic trajectory. The circles indicate the populated state at a given time. The insets show the electron density difference of the S_1 and S_0 states with areas of depletion (increase) of electron density in S_1 shown in red (blue). The character of the S_1 state changes from ππ* (left) to intra-CT (middle) and inter-CT (right). The switch from intra-CT to inter-CT state at 203 fs is followed by ultrafast population transfer to the ground state. The time scale of relaxation is underestimated due to the over stabilization of charge transfer states by TDDFT. (b) The N···O distance along the trajectory. The computations have been performed at the PBE0/SVP//GAFF level, for details see Computational Methods.

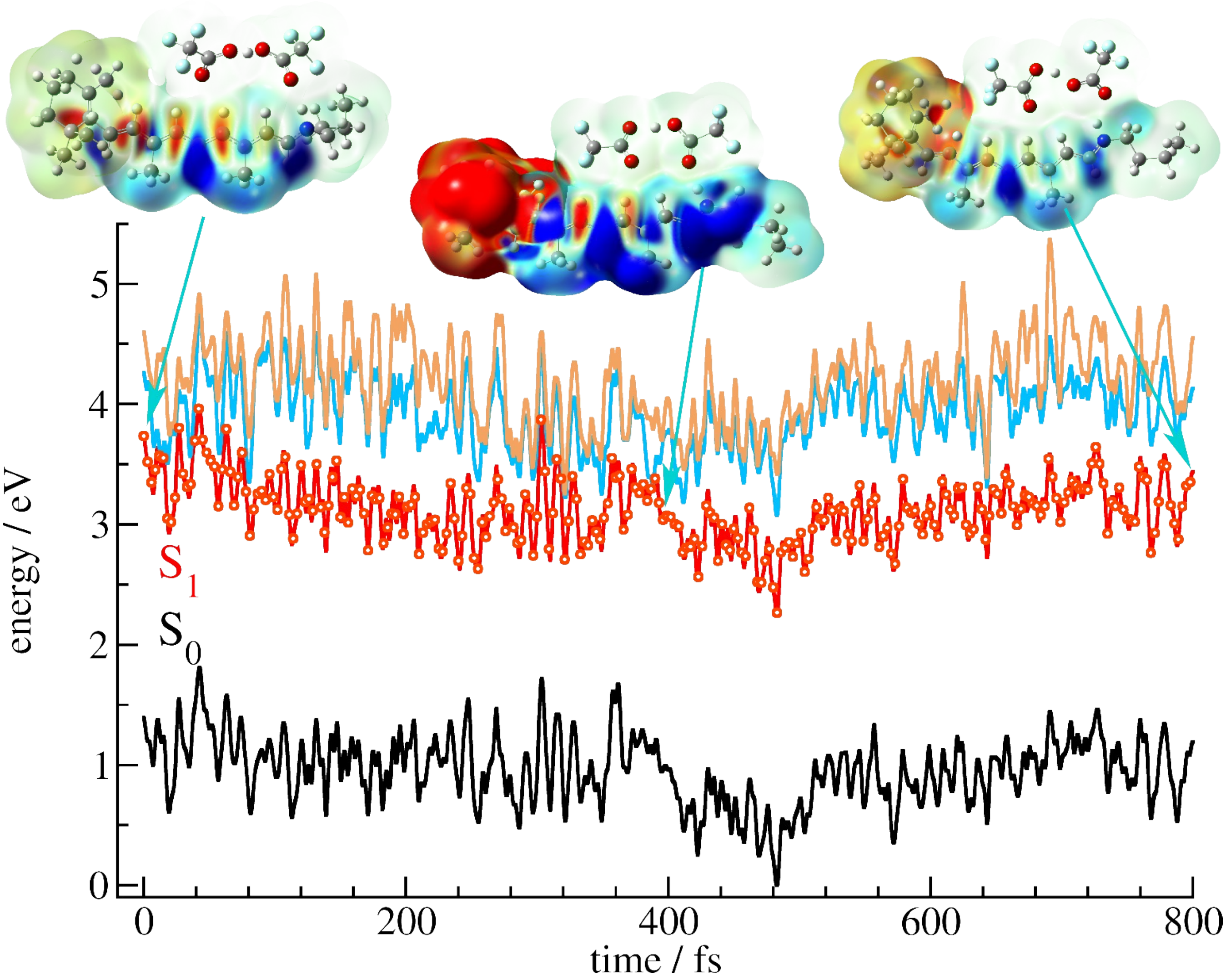

Figure S15. Time dependence of the potential energy of the electronic ground state (S_0, black) and the first three excited singlet states (S_1, red; S_2, blue; S_3 ocher) for a selected nonadiabatic trajectory that has not deactivated to the ground state. The circles indicate the populated state at a given time. The insets show the electron density difference of the S_1 and S_0 states with areas of depletion (increase) of electron density in S_1 shown in red (blue). The main geometrical changes along non-deactivated trajectories includes deformations of the conjugated backbone, rotation of the β-ionone ring and increase of the flexibility of the *n*-butyl tail.

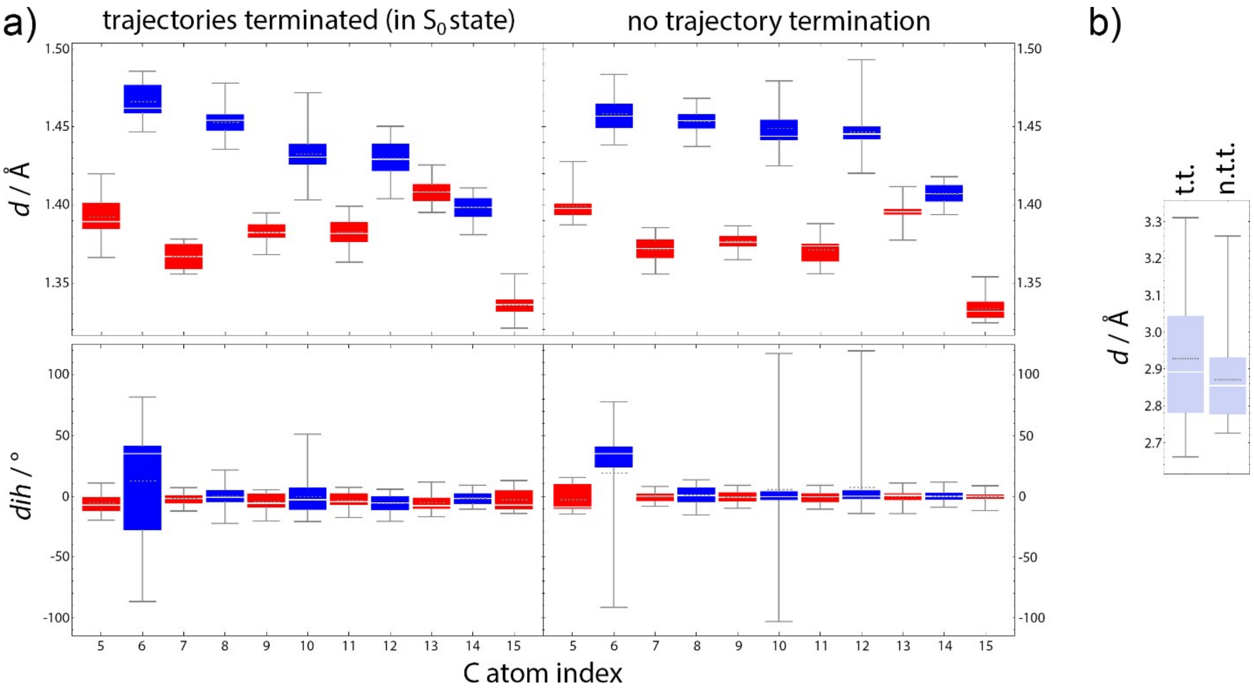

Figure S16. a) Box-and-whisker distribution plots for the most representative internal coordinates of the conjugated PSBR$^+$ chain average for each trajectory and categorized into a set of trajectories that terminate in the ground electronic state through the intra-/inter-CT (left) CI and those which do not terminate in the 800 fs simulation time (right). The top row figures show in red (blue) double (single) C_iC_{i+1} bond distances designated using the same atom designations as in Figure 1a of article, while the bottom figures the relative change of the torsional angle between the same C_iC_{i+1} (defined as $C_{i-1}C_iC_{i+1}C_{i+2}$) from their corresponding in-plane values. The upper (lower) whiskers designate the maximum (minimum) average value, while the box edges designate the first and third distribution quartile, the white horizontal line the distribution median and the distribution mean with a black dotted line. b) Box-and-whisker distribution plots for the N-H···O hydrogen bond distance between PSBR$^+$ and TFA$^-$ for the same two sets of trajectories.

S_1: 453.9 nm

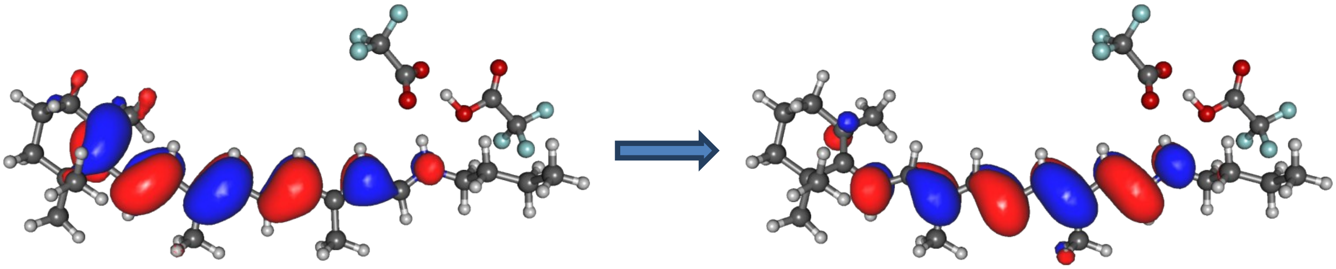

S_2: 310.7 nm

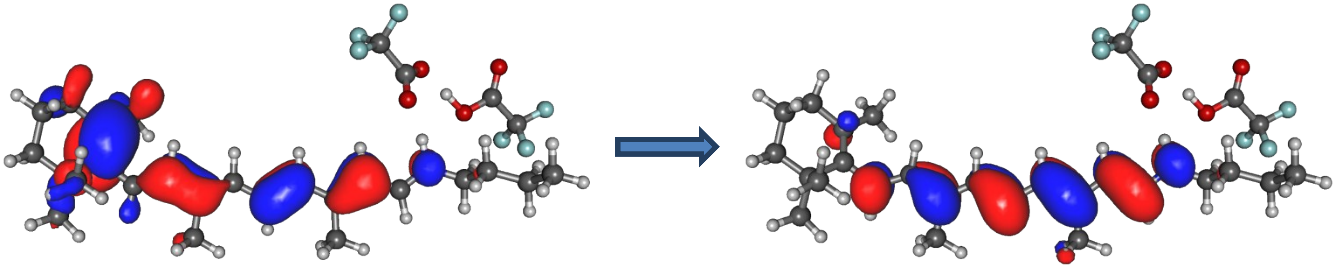

Figure S17: The main orbital contributions to the two lowest singlet excited states of 6-*cis* [*n*SBR$^+$TFA$^-$]TFA in DCM. ADC(2)/cc-pVDZ//MP2/cc-pVDZ COSMO(DCM).

S_1: 450.0 nm

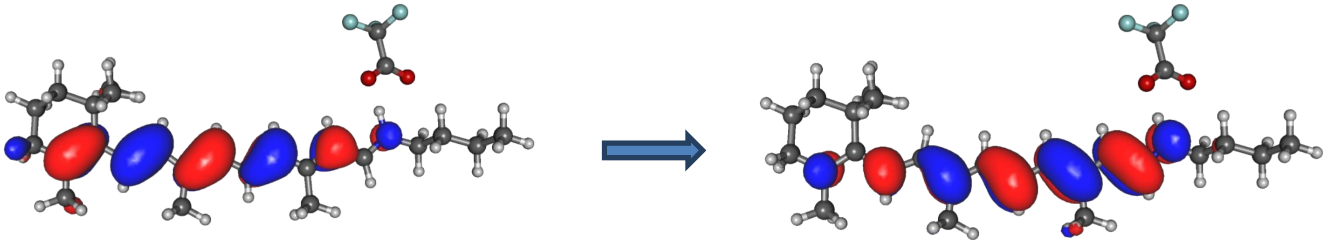

S_2: 294.4 nm

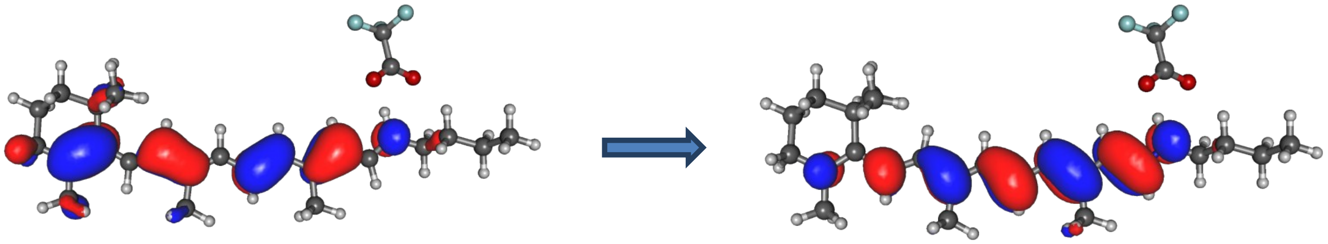

Figure S18: The main orbital contributions to the two lowest singlet excited states of 6-*trans* [*n*SBR$^+$TFA$^-$] in DCM. ADC(2)/cc-pVDZ//MP2/cc-pVDZ COSMO(DCM).

S_1: 421.2 nm

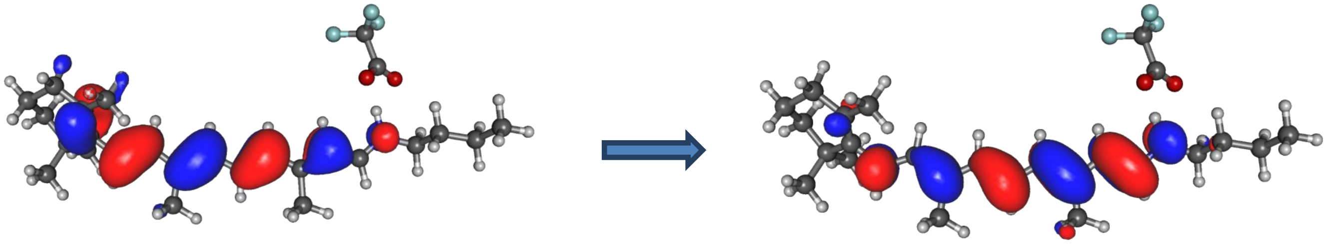

S_2: 297.3 nm

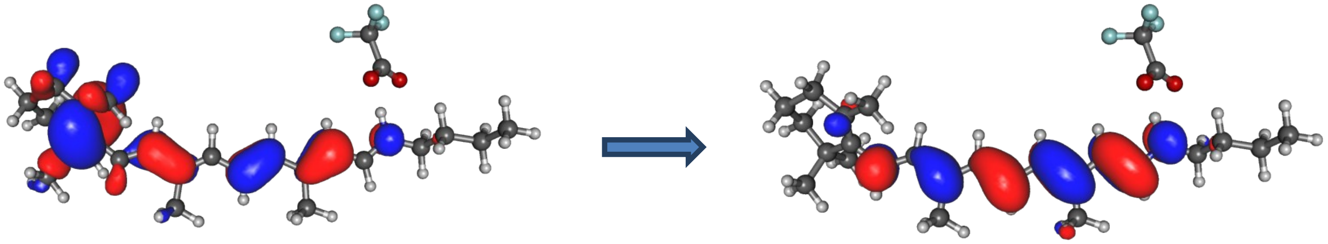

Figure S19: The main orbital contributions to the two lowest singlet excited states of 6-*cis* [*n*SBR$^+$TFA$^-$] in DCM. ADC(2)/cc-pVDZ//MP2/cc-pVDZ COSMO(DCM).

Table S2. Geometry of the S_0 minimum of 6-*cis* [*n*SBR$^+$TFA$^-$]TFA in DCM. MP2/cc-pVDZ COSMO(DCM).

C	-8.151163	1.550684	-0.647615
C	-8.287745	0.214562	-0.368788
C	-9.561495	-0.375154	0.253752
C	-10.692933	0.667913	0.293947
C	-10.203669	2.035275	0.756819
C	-9.203204	2.566876	-0.263862
C	-7.214751	-0.756394	-0.639016
C	-5.889716	-0.553503	-0.365701
C	-4.828314	-1.519298	-0.614434
C	-5.197916	-2.865359	-1.182607
C	-10.066979	-1.570856	-0.575961
C	-9.239217	-0.870389	1.675612
C	-6.984551	2.155185	-1.391551
C	-3.535423	-1.146796	-0.309197
C	-2.348626	-1.949259	-0.455836
C	-1.100516	-1.475011	-0.132494
C	0.128019	-2.238505	-0.244628
C	0.045257	-3.666118	-0.721100
C	1.303671	-1.605432	0.097371
C	2.596087	-2.224456	0.032126
N	3.687590	-1.585756	0.343344
C	5.015979	-2.195249	0.367463
C	5.524161	-2.276468	1.807802
C	6.933560	-2.865923	1.885879
C	7.427573	-2.982854	3.328027
O	3.176240	0.877093	1.231666
C	3.370946	2.012580	0.733718
O	4.200937	2.391891	-0.136467
C	2.478932	3.156572	1.260665
F	3.213028	4.031919	1.980407
F	1.917660	3.842047	0.244588
F	1.484763	2.717101	2.049104
H	-11.118717	0.773700	-0.722416
H	-11.501106	0.286242	0.943518
H	-9.717882	1.950760	1.744750
H	-11.046170	2.737811	0.870864
H	-8.689691	3.467584	0.121990
H	-9.731649	2.893821	-1.182810
H	-9.400331	-2.444842	-0.503520
H	-10.173922	-1.296339	-1.638831
H	-11.057390	-1.880679	-0.198976
H	-8.413097	-1.601236	1.652628
H	-10.122135	-1.361248	2.121705
H	-8.933187	-0.039157	2.331907
H	-6.396581	1.409170	-1.944708
H	-6.303711	2.687736	-0.702907
H	-7.363379	2.909940	-2.103302

H	-7.512737	-1.731973	-1.038599
H	-5.584691	0.395449	0.092969
H	-3.389246	-0.135497	0.094285
H	-2.447649	-2.971750	-0.832918
H	-1.010811	-0.445301	0.237353
H	1.272229	-0.569439	0.452584
H	2.714375	-3.265378	-0.286331
H	-4.326137	-3.515669	-1.330246
H	-5.705263	-2.746648	-2.154544
H	-5.902303	-3.381935	-0.509212
H	1.017665	-4.171555	-0.753304
H	-0.391062	-3.700136	-1.732207
H	-0.617812	-4.243108	-0.056906
H	3.601466	-0.577901	0.659600
H	4.943243	-3.192698	-0.093330
H	5.674332	-1.563943	-0.243776
H	5.517105	-1.262696	2.247614
H	4.823250	-2.891652	2.400352
H	6.936034	-3.862699	1.409274
H	7.622743	-2.233441	1.300850
H	8.442431	-3.408933	3.369960
H	7.453603	-1.993312	3.813780
H	6.761035	-3.631957	3.919798
H	5.148859	1.416652	-0.613359
O	5.817830	0.697615	-0.998309
C	7.036353	1.189889	-1.011934
O	7.421576	2.281811	-0.637608
C	8.015609	0.167543	-1.619124
F	7.989589	-0.998483	-0.933600
F	7.687188	-0.109667	-2.893757
F	9.269438	0.625822	-1.599277

Table S3. Geometry of the S_0 minimum of 6-*trans* [*n*SBR$^+$TFA$^-$] in DCM. MP2/cc-pVDZ COSMO(DCM).

C	-6.851892	1.448690	0.686958
C	-8.231260	2.068117	0.995343
C	-9.234984	1.867963	-0.132138
C	-9.500536	0.374851	-0.277804
C	-8.245033	-0.465253	-0.253422
C	-7.013070	0.026871	0.126642
C	-8.472603	-1.885187	-0.733449
C	-5.857098	-0.860751	-0.024896
C	-4.517198	-0.576547	0.053523
C	-3.463176	-1.558121	-0.153886
C	-3.837949	-2.988415	-0.451874
C	-6.087084	1.423864	2.025782
C	-6.115821	2.360810	-0.315105
C	-2.158663	-1.118165	-0.068777
C	-0.966344	-1.906252	-0.241670
C	0.289474	-1.358871	-0.155898
C	1.529211	-2.092475	-0.336730
C	1.456312	-3.572920	-0.613210
C	2.703823	-1.379689	-0.254423
C	4.015283	-1.941848	-0.446997
N	5.083705	-1.206891	-0.364525
C	6.434294	-1.729097	-0.543612
C	7.172690	-1.777760	0.794461
C	8.586117	-2.341604	0.637206
C	9.332733	-2.404955	1.969698
H	-8.635954	1.595962	1.910792
H	-8.086198	3.139104	1.222696
H	-8.837321	2.272846	-1.078680
H	-10.173454	2.407202	0.079200
H	-10.041985	0.158720	-1.217897
H	-10.169502	0.024519	0.534746
H	-5.030684	1.142483	1.919644
H	-6.561300	0.715865	2.725832
H	-6.122505	2.430107	2.479161
H	-5.118070	1.978036	-0.573290
H	-5.989405	3.367279	0.121844
H	-6.684628	2.461615	-1.253199
H	-7.888570	-2.634425	-0.179182
H	-8.224643	-1.988850	-1.805048
H	-9.536752	-2.146457	-0.619745
H	-6.101400	-1.895286	-0.280331
H	-4.171467	0.437662	0.266967
H	-2.007892	-0.052222	0.151503
H	-1.066797	-2.975011	-0.454146
H	0.380145	-0.284490	0.051392
H	2.659672	-0.304558	-0.046218
H	4.148996	-3.003989	-0.683469

H	-2.960120	-3.637021	-0.568501
H	-4.430304	-3.045941	-1.380527
H	-4.462475	-3.401538	0.357782
H	2.442501	-4.042037	-0.715044
H	0.890547	-3.755407	-1.541319
H	0.919701	-4.080078	0.204885
H	4.965702	-0.128375	-0.128658
H	6.365466	-2.732725	-0.992855
H	6.949734	-1.045306	-1.233644
H	7.215296	-0.759466	1.220653
H	6.597338	-2.406267	1.498094
H	8.524063	-3.353093	0.196055
H	9.150358	-1.718227	-0.079403
H	10.338383	-2.836340	1.845498
H	9.444852	-1.398173	2.404028
H	8.784684	-3.025700	2.697495
O	4.711677	1.288214	0.136838
C	5.674457	1.922516	-0.407138
O	6.681432	1.483437	-0.986477
C	5.582801	3.461150	-0.294059
F	4.386913	3.898866	0.139952
F	6.515050	3.921436	0.572931
F	5.820351	4.056005	-1.482138

Table S4. Geometry of the S_0 minimum of 6-*cis* [*n*SBR$^+$TFA$^-$] in DCM. MP2/cc-pVDZ COSMO(DCM).

C	5.747479	2.674790	3.306043
C	7.262288	2.674900	3.306411
C	7.871316	4.074556	3.306205
C	7.163028	4.931118	2.262723
C	5.667758	5.118350	2.573668
C	4.995215	5.693877	1.315110
H	3.938710	5.950518	1.494159
H	5.035935	4.968550	0.484808
H	5.521445	6.612079	0.999997
C	5.488740	6.119289	3.731046
H	4.422379	6.275266	3.964326
H	5.916263	7.098984	3.452813
H	5.987696	5.770008	4.649148
H	7.260466	4.438251	1.276429
H	7.633452	5.927093	2.173782
H	7.760569	4.526855	4.306978
H	8.952775	4.019829	3.096286
H	7.617854	2.097678	4.178886
H	7.610859	2.114037	2.415155
C	5.139731	1.358841	3.730116
H	4.070182	1.440344	3.967571
H	5.673483	0.973129	4.615991
H	5.254853	0.597769	2.936449
C	5.018215	3.777994	2.946214
C	3.543332	3.782529	2.921038
H	3.044154	4.648592	3.374176
C	2.770603	2.839643	2.302466
H	3.272439	2.010822	1.786713
C	1.314138	2.850380	2.237976
C	0.571543	3.970950	2.920050
H	0.872473	4.944341	2.497077
H	0.817449	3.995796	3.994782
H	-0.517848	3.878484	2.820483
C	0.694765	1.830791	1.546717
H	1.345011	1.071285	1.091281
C	-0.722498	1.653075	1.346513
H	-1.412437	2.383189	1.780860
C	-1.230732	0.601768	0.624289
H	-0.528401	-0.123701	0.193102
C	-2.642711	0.368131	0.370546
C	-3.648378	1.335712	0.940353
H	-4.685102	1.073081	0.696052
H	-3.452007	2.351199	0.560576
H	-3.554206	1.372088	2.037595
C	-2.974781	-0.732200	-0.386170
H	-2.173608	-1.382153	-0.755957
C	-4.315091	-1.110438	-0.757500

H	-5.183577	-0.507914	-0.466922
N	-4.529448	-2.177379	-1.466881
H	-3.658811	-2.798200	-1.776102
C	-5.846235	-2.626626	-1.903980
H	-6.597430	-1.872572	-1.619123
H	-5.798865	-2.704121	-3.001348
C	-6.162380	-3.994047	-1.297292
H	-5.343970	-4.691104	-1.551497
H	-6.184998	-3.904616	-0.196404
C	-7.493108	-4.551308	-1.805425
H	-8.303589	-3.841249	-1.560914
H	-7.457370	-4.623991	-2.907038
C	-7.809468	-5.922004	-1.206101
H	-8.768961	-6.311105	-1.581862
H	-7.022904	-6.651161	-1.461407
H	-7.872573	-5.864009	-0.106864
O	-2.481901	-3.537603	-2.198734
C	-2.600143	-3.657948	-3.466288
O	-3.563233	-3.382404	-4.196092
C	-1.321358	-4.222250	-4.124553
F	-1.463392	-4.426090	-5.445759
F	-0.280690	-3.373722	-3.959516
F	-0.960682	-5.401415	-3.572432

Table S6. S2/S1 CI geometry from LIP presented in Figure 5.

C	5.547076	4.622804	-2.483520
C	6.920331	4.591233	-3.125007
C	6.905280	5.010965	-4.594312
C	5.785138	4.264834	-5.313525
C	4.392407	4.622804	-4.761016
C	3.396621	3.564706	-5.274546
H	2.357571	3.808697	-5.000018
H	3.636481	2.572820	-4.852174
H	3.455738	3.500558	-6.376978
C	3.960468	6.008576	-5.282025
H	2.954850	6.280068	-4.919959
H	3.924871	6.001205	-6.387054
H	4.657933	6.799063	-4.957504
H	5.949910	3.176697	-5.187017
H	5.798338	4.467121	-6.401360
H	6.740813	6.101417	-4.664777
H	7.881207	4.799942	-5.067295
H	7.599207	5.241497	-2.541611
H	7.337991	3.566419	-3.031546
C	5.573725	4.660677	-0.972671
H	4.605800	4.953085	-0.539971
H	6.349379	5.369312	-0.628633
H	5.849795	3.674361	-0.552850
C	4.392407	4.622804	-3.224377
C	3.051344	4.659781	-2.615138
H	2.331609	5.364743	-3.053053
C	2.607944	3.806419	-1.635388
H	3.304649	3.033470	-1.276978
C	1.280623	3.784150	-1.059613
C	0.284007	4.868425	-1.396108
H	-0.368478	4.570503	-2.237979
H	0.791441	5.804130	-1.678572
H	-0.369088	5.092455	-0.536189
C	0.921365	2.697663	-0.260430
H	1.695323	1.932727	-0.085880
C	-0.351455	2.472735	0.314478
H	-1.127330	3.236628	0.184103
C	-0.674372	1.281188	1.003339
H	0.120247	0.519006	1.050959
C	-1.888354	0.960242	1.616332
C	-3.034812	1.937520	1.703448
H	-3.346371	2.090253	2.753025
H	-3.916817	1.560895	1.154385
H	-2.770793	2.920296	1.286666
C	-2.038603	-0.341438	2.221455
H	-1.186462	-1.032979	2.129260
C	-3.140961	-0.764762	2.925156

H	-4.017544	-0.119334	3.060700
N	-3.216713	-1.984862	3.565124
H	-2.464539	-2.649310	3.329850
C	-4.476821	-2.561047	3.995023
H	-5.136046	-1.742197	4.336175
H	-5.001585	-3.073970	3.159198
C	-4.224753	-3.544075	5.138679
H	-3.576755	-4.363160	4.771183
H	-3.654015	-3.017383	5.923668
C	-5.498533	-4.143284	5.736301
H	-6.162214	-3.322985	6.064524
H	-6.045437	-4.701560	4.952128
C	-5.192124	-5.063864	6.920816
H	-6.108935	-5.496043	7.353976
H	-4.536832	-5.898436	6.614040
H	-4.675782	-4.505733	7.719739
O	-2.167487	-4.575621	2.153564
C	-2.562863	-5.669447	1.641018
O	-3.321665	-6.354597	2.380254
C	-2.298933	-6.013528	0.174792
F	-2.802970	-5.075590	-0.627380
F	-0.977122	-6.093197	-0.038697
F	-2.853395	-7.192654	-0.120178